

Instability of a charged non-Newtonian liquid jet

An-Cheng Ruo,¹ Kuan-Hung Chen,¹ Min-Hsing Chang,² and Falin Chen^{1,*}

¹*Institute of Applied Mechanics, National Taiwan University, Taipei 106, Taiwan*

²*Department of Mechanical Engineering, Tatung University, Taipei 104, Taiwan*

(Received 18 August 2011; published 9 January 2012)

A three-dimensional instability analysis of an electrified non-Newtonian liquid jet is performed in this paper so as to understand the competition between viscoelastic stresses, electric force, and surface tension. The analysis employs the leaky-dielectric model to account for the charge transport process and the Oldroyd-B model to take the viscoelastic effect into account. Results show that the viscoelastic stresses play a stabilizing role while electrification destabilizes the disturbances with shorter wavelength and higher azimuthal wave numbers. However, the viscoelastic stabilizing effect is not so significant on the sinuous mode (with azimuthal wave number $m = 1$) compared with the other modes, which thus promotes sinuous disturbances. This result is consistent with the presence of bending motion in most experimental observations.

DOI: [10.1103/PhysRevE.85.016306](https://doi.org/10.1103/PhysRevE.85.016306)

PACS number(s): 47.50.-d, 47.85.Dh, 47.60.Kz

I. INTRODUCTION

A charged liquid jet subjected to electrical instability has been known to be more unstable than an uncharged jet. The electrostatic repulsive force caused by free charges on the jet surface tends to trigger the growth of nonaxisymmetric disturbances with shorter wavelength than those in the uncharged cases, causing the breakup into atomized droplets [1]. This related technique is widely applied to electrostatic spray [2] for industrial or agricultural purposes.

The theoretical work was pioneered by Rayleigh [3], who developed a theory of stability for electrified inviscid jets moving in vacuum subjected to disturbances of infinite wavelength. Basset [4] studied the stability of axisymmetric disturbances on charged Newtonian jets taking the effects of viscosity and the ambient gas into account. Errors in Basset's analysis were later corrected by Taylor [5]. Schneider *et al.* experimentally verified the axisymmetric theoretical results by observing the breakup of a charged water jet through a grounded cylindrical electrode [6]. Huebner conducted a series of experiments of charged water jets and showed that increasing the amount of electrical charge enhances the growth of sinuous nonaxisymmetric disturbances [7]. Particularly, when using isopropyl alcohol instead of distilled water, he observed that at sufficiently high electrification, the circular jet may develop a fanlike configuration [8]. To explain the phenomena associated with nonaxisymmetric motions, Huebner developed the Lagrangian equation of motion to analyze the three-dimensional instability of charged inviscid jets with arbitrary wave number [9]. His analysis elucidated how the electrical force amplifies short-wavelength disturbances and stabilizes the long waves driven by surface tension. Nevertheless, the axisymmetric varicose mode is found to be predominant for all cases, which thus cannot explain the sinuous motion observed in experiments. Saville [10] took the fluid viscosity into account and found that the viscous damping effect provides significant resistance to the growth of axisymmetric disturbances more than that of the sinuous

one. At a sufficiently high ratio of viscous to electrical forces, the sinuous mode may prevail over the axisymmetric one, which successfully explains the bending instability observed in experiments.

So far in most theoretical studies of electrified jets, the liquid is usually assumed to be a perfect conductor with equipotential surface and zero electric field in the bulk. This assumption, however, could have overestimated the growth rate of disturbances. In fact, the assumption of perfect conductor can hold only when the electrical relaxation time is much shorter than the hydrodynamic characteristic time. For example, the ratio of characteristic time to electrical relaxation time for water jets is usually as large as 10^4 , even in the last stages of pinch-off. However, in many practical applications, such as food and pharmacy technologies, the liquid used is usually of poor conductivity, allowing free charges to persist in the fluid bulk, inducing electrical body forces to affect the flow motion. Furthermore, the interfacial electric stresses are no longer perpendicular to the jet surface because the surface of the imperfect conducting liquid is not equipotential. For such a liquid, the Taylor-Melcher leaky-dielectric model is appropriate for the description of the relaxation process of free charges [11,12]. Recently, this model has been extensively used in subsequent studies. For example, López-Herrera *et al.* [13] performed an axisymmetric instability analysis for a leaky-dielectric liquid jet flowing through a coaxial grounded electrode; Li *et al.* [14,15] investigated the instability of electrified compound jets of which the outer liquid is considered to be a leaky dielectric, and Ruo *et al.* [16] studied the stability of charged semiconducting jets in the presence of axial magnetic field.

In ink-jet printing technology, polymeric materials are usually added in the ink solution to change the physical and chemical properties [17,18]. This motivates us to extend the study toward that of viscoelastic jets. However, unlike a vast amount of literature on the study of Newtonian fluid jets, the theoretical work of viscoelastic jets is relatively limited. The main reason for this is the mathematical difficulty in dealing with nonlinear rheological constitutive equations. Incipient studies on the instability of non-Newtonian jets [19–24] showed that a viscoelastic jet is always less stable

*falin@spring.iam.ntu.edu.tw

than its Newtonian counterpart and the elastic force plays a destabilizing role on the onset of instability, whatever form of rheological constitutive equation is used [23,24]. However, this result disagrees with most experimental evidence because the addition of polymers generally stabilizes the jet and delays the breakup due to high extensional viscosities. In particular, once the strain-hardening effect prevails over the pinching effect caused by surface tension, the jet will not break up at all, forming a “beads-on-string” structure observed in experiments. To resolve this discrepancy, Goren and Gottlieb [25] first suggested that for a viscoelastic liquid ejected from a capillary tube subject to hydrodynamic pressure, the elastic stresses generated at the nozzle due to the stretching of entangled polymeric chains can persist along the jet for a long distance downstream far from the exit, which may provide a resistance to the instability of viscoelastic jets. With such a concept, Goren and Gottlieb demonstrated how the presence of unrelaxed axial tension suppresses the surface-tension-driven instability. Later, Bousfield *et al.* [26] also followed this concept to perform a numerical simulation of axisymmetric deformation of a viscoelastic cylindrical column to confirm that the unrelaxed tension indeed provides significant resistance to instability, thereby delaying the breakup time.

The present work aims to examine the three-dimensional instability of a charged non-Newtonian liquid jet by considering the interaction between electric force and viscoelastic stresses. This subject is of fundamental importance to the understanding of the instability phenomena occurring in continuous ink-jet printing or electrospinning processes. Despite the nonlinear nature of most of the phenomena, the linear features appearing upstream provide important information for the subsequent behaviors developing downstream. In the following sections, we first develop a mathematical formulation to describe the three-dimensional motion of a charged viscoelastic jet subjected to electrical forces, surface tension, aerodynamic interaction, and viscoelastic stresses. The leaky-dielectric model is adopted to account for the effects of finite electrical relaxation time as well as nonzero tangential electric stresses at the jet surface, and the Oldroyd-B model [27] is used to describe the viscoelastic effect due to the presence of polymeric molecules. Then we use normal mode analysis to linearize the governing equations and yield a nonlinear eigenvalue problem, which is solved by employing the Chebyshev collocation method [28] with a matrix transformation. Finally, the instability mechanisms are elucidated by depicting a series of dispersion diagrams.

II. FORMULATION OF THE PROBLEM

A. Governing equations

Consider a charged capillary viscoelastic jet of radius a , density ρ , electrical conductivity σ , and permittivity ε , moving at a uniform velocity U through a quiescent surrounding gas of density ρ_a . A schematic description of system configuration is shown in Fig. 1. For an incompressible isothermal liquid of arbitrary rheology in the presence of electrostatic field, the equations governing the conservation of mass and momentum

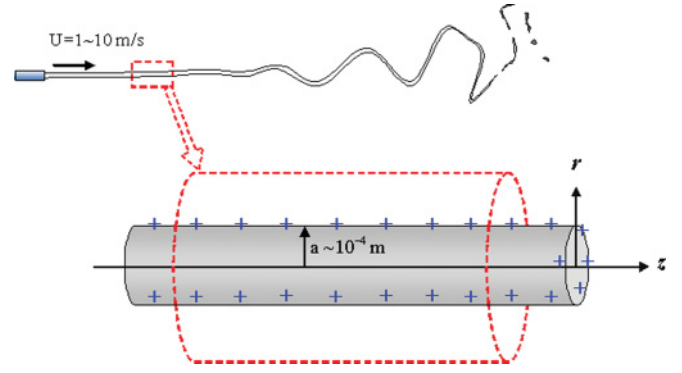


FIG. 1. (Color online) A schematic description of local instability analysis for a charged viscoelastic jet ejected by hydrodynamic pressure from a capillary tube. The onset of instability occurs in the segment circled by the dashed line.

in terms of cylindrical coordinates (r, θ, z) can be acquired according to references [11,12,27]:

$$\frac{1}{r} \frac{\partial}{\partial r}(ru_r) + \frac{1}{r} \frac{\partial u_\theta}{\partial \theta} + \frac{\partial u_z}{\partial z} = 0, \quad (1)$$

$$\begin{aligned} \rho \left(\frac{\partial u_r}{\partial t} + u_r \frac{\partial u_r}{\partial r} + u_\theta \frac{\partial u_r}{r \partial \theta} + u_z \frac{\partial u_r}{\partial z} - \frac{u_\theta^2}{r} \right) \\ = -\frac{\partial P}{\partial r} - q \frac{\partial \phi}{\partial r} + \frac{1}{r} \frac{\partial}{\partial r}(r\tau_{rr}) + \frac{\partial \tau_{\theta r}}{r \partial \theta} + \frac{\partial \tau_{zr}}{\partial z} - \frac{\tau_{\theta\theta}}{r}, \end{aligned} \quad (2)$$

$$\begin{aligned} \rho \left(\frac{\partial u_\theta}{\partial t} + u_r \frac{\partial u_\theta}{\partial r} + u_\theta \frac{\partial u_\theta}{r \partial \theta} + u_z \frac{\partial u_\theta}{\partial z} + \frac{u_\theta u_r}{r} \right) \\ = -\frac{\partial P}{r \partial \theta} - q \frac{\partial \phi}{r \partial \theta} + \frac{1}{r^2} \frac{\partial}{\partial r}(r^2 \tau_{r\theta}) \\ + \frac{\partial \tau_{\theta\theta}}{r \partial \theta} + \frac{\partial \tau_{z\theta}}{\partial z} + \frac{\tau_{\theta r} - \tau_{r\theta}}{r}, \end{aligned} \quad (3)$$

$$\begin{aligned} \rho \left(\frac{\partial u_z}{\partial t} + u_r \frac{\partial u_z}{\partial r} + u_\theta \frac{\partial u_z}{r \partial \theta} + u_z \frac{\partial u_z}{\partial z} \right) \\ = -\frac{\partial P}{\partial z} - q \frac{\partial \phi}{\partial z} + \frac{1}{r} \frac{\partial}{\partial r}(r\tau_{rz}) + \frac{\partial \tau_{\theta z}}{r \partial \theta} + \frac{\partial \tau_{zz}}{\partial z}, \end{aligned} \quad (4)$$

where $\mathbf{V} = u_r \mathbf{e}_r + u_\theta \mathbf{e}_\theta + u_z \mathbf{e}_z$ is the velocity field, P is the pressure, q is the volumetric density of free charges, ϕ is the electrical potential, and τ_{ij} with the subscripts $i, j = r, \theta, z$ represents the components of viscoelastic stress tensor $\boldsymbol{\tau}$.

The electrical potential ϕ is governed by Poisson's equation:

$$\nabla^2 \phi = \frac{\partial^2 \phi}{\partial r^2} + \frac{\partial \phi}{r \partial r} + \frac{\partial^2 \phi}{r^2 \partial \theta^2} + \frac{\partial^2 \phi}{\partial z^2} = -\frac{q}{\varepsilon}. \quad (5)$$

The conservation of free charges obeying Ohmic law is

$$\frac{Dq}{Dt} = \frac{\partial q}{\partial t} + u_r \frac{\partial q}{\partial r} + u_\theta \frac{\partial q}{r \partial \theta} + u_z \frac{\partial q}{\partial z} = -\frac{\sigma}{\varepsilon} q. \quad (6)$$

For the rheological relation between $\boldsymbol{\tau}$ and \mathbf{V} , we employ the Oldroyd-B equation, which is the simplest constitutive equation useful for describing dilute polymer solutions at high

rates of deformation [27,29]:

$$\begin{aligned} \boldsymbol{\tau} + \lambda_1 \left[\frac{\partial \boldsymbol{\tau}}{\partial t} + \mathbf{V} \cdot \nabla \boldsymbol{\tau} - (\nabla \mathbf{V})^T \cdot \boldsymbol{\tau} - \boldsymbol{\tau} \cdot \nabla \mathbf{V} \right] &= \mu \dot{\boldsymbol{\gamma}} \\ + \mu \lambda_2 \left[\frac{\partial \dot{\boldsymbol{\gamma}}}{\partial t} + \mathbf{V} \cdot \nabla \dot{\boldsymbol{\gamma}} - (\nabla \mathbf{V})^T \cdot \dot{\boldsymbol{\gamma}} - \dot{\boldsymbol{\gamma}} \cdot \nabla \mathbf{V} \right], \end{aligned} \quad (7)$$

where λ_1 is the stress relaxation time, λ_2 is the deformation retardation time, μ is the zero-shear-rate viscosity, and $\dot{\boldsymbol{\gamma}} = \nabla \mathbf{V} + (\nabla \mathbf{V})^T$ is the rate-of-strain tensor. The use of the Oldroyd-B model implies that the present analysis is valid only for Boger fluids, which are known as a kind of liquid with constant shear viscosity and different degrees of elasticity [30–33]. In many academic researches, the employment of Boger fluids has the advantage of removing the mask of the non-Newtonian viscous effects (e.g., shear thinning), so as to exclusively manifest the elastic effects on the flow stability of viscoelastic liquids [30]. For example, Mun *et al.* [34] conducted a series of experiments using Boger fluids to investigate the elastic effect on the instability and breakup of uncharged capillary jets. Yu *et al.* [35] investigated the role of elasticity in the formation of electrospun fibers for a series of solutions having the same surface tension, zero-shear viscosity, and conductivity but different degrees of elasticity.

As for the surrounding gas, the governing equations are basically the same as Eqs. (1)–(7) except that the viscoelastic stress tensor $\boldsymbol{\tau}$ and free charge density q disappear since both viscosity and conductivity of the gas are neglected in this analysis. Note that the inviscid assumption of the gas allows the basic flow profile to be flat, thus simplifying the present analysis. However, this assumption restricts the scope to the flow configuration in the first wind-induced regime, where the effect of viscous boundary layer at the jet surface is negligible and the aerodynamic interaction is accounted for only in terms of pressure fluctuation [13].

B. Boundary conditions

The boundary conditions at the interface between the liquid and the gas, $r = R(\theta, z, t)$, are described as follows. First, the kinematic condition at the interface is

$$\frac{D}{Dt} [r - R(\theta, z, t)] = 0, \quad (8)$$

and the normal and tangential stress balances at the interface are described by

$$\mathbf{n} \cdot (-P_a \mathbf{I} - \mathbf{T}) \cdot \mathbf{n} = \gamma \nabla \cdot \mathbf{n}, \quad (9)$$

$$\mathbf{n} \cdot \mathbf{T} \cdot \mathbf{t} = \nabla \gamma \cdot \mathbf{t}, \quad (10)$$

where the subscript “ a ” denotes the physical quantities of the gas, γ is the surface tension coefficient, \mathbf{I} is the identity matrix, \mathbf{n} and \mathbf{t} denote the unit vectors normal and tangential to the interface, and \mathbf{T} is the stress tensor. Note that since no temperature gradient is considered in the present problem, the surface tension gradient is zero and the right-hand term of Eq. (10) disappears. For flows in quasistatic electric fields, the stress tensor \mathbf{T} consists of mechanical and electrostatic Maxwell stress tensors [12]:

$$\mathbf{T} = -P\mathbf{I} + \boldsymbol{\tau} + \varepsilon(\nabla\phi\nabla\phi - \frac{1}{2}|\nabla\phi|^2\mathbf{I}). \quad (11)$$

The electric conditions at the interface are

$$(\varepsilon\nabla\phi - \varepsilon_a\nabla\phi_a) \cdot \mathbf{n} = Q, \quad (12)$$

$$\nabla\phi \cdot \mathbf{t} = \nabla\phi_a \cdot \mathbf{t}, \quad (13)$$

where ε_a is the permittivity in vacuum, and $Q = Q(\theta, z, t)$ is the surface charge density, which must satisfy the conservation of charge at the interface:

$$\frac{\partial Q}{\partial t} + [\nabla - \mathbf{n}(\mathbf{n} \cdot \nabla)] \cdot \mathbf{K} + \sigma \nabla\phi \cdot \mathbf{n} = 0, \quad (14)$$

where \mathbf{K} is surface current density [11,12]. For an imperfect conducting fluid, the surface current due to conduction is negligible, and hence the contribution from the current transported by the fluid motion will be dominant (i.e., $\mathbf{K} \approx Q\mathbf{V}$) [16].

III. LINEAR INSTABILITY ANALYSIS

A. Base-state solutions

Before the onset of instability, the jet is assumed to be perfectly cylindrical and the velocity is axisymmetric (i.e., plug flow) and unidirectional with an axial elastic tension $\bar{\tau}_{zz}$ retained as shown in Fig. 1. In such a condition, no free charge exists in the bulk of the jet or in the gas (i.e., $\bar{q} = 0$) and the charges uniformly distribute on the jet surface with a surface charge density Q_0 . Solving Eq. (5) based on this state, the electrical potentials of the liquid and the gas can be obtained as

$$\bar{\phi}(r) = \varphi_0, \quad (15)$$

$$\bar{\phi}_a(r) = -\frac{Q_0 a}{\varepsilon_a} \ln \frac{r}{a} + \varphi_0, \quad (16)$$

where φ_0 is the electrical potential applied on the jet surface. On the other hand, the constitutive Eq. (7) can be solved to obtain the base-state elastic tension:

$$\bar{\tau}_{zz}(z) = \bar{\tau}_{zz}(0) \exp(-z/\lambda_1 U), \quad (17)$$

which implies that the elastic tension will eventually fade away downstream. However, the presence of the spatial dependence on the base-state solution makes the subsequent analysis difficult. A simplification is necessary for further analysis. Following the approach proposed by Goren and Gottlieb [25], we focus the analysis on a segment of the jet where the elastic tension can be assumed to be constant (i.e., $\bar{\boldsymbol{\tau}} \approx \tau_0 \mathbf{e}_z \mathbf{e}_z$). This assumption is valid only if $\lambda_1 \gg L/U$ (where L is the wavelength of a disturbance). This inequality, in terms of the dimensionless parameters introduced in Table I, can be rewritten as $De \gg 2\pi/k$. This means that to neglect the spatial dependence of the basic-state solution, the analysis must be limited at high Deborah number.

B. Linearization and normal mode analysis

The governing equations are nondimensionalized using the quantities a , U , a/U , $Q_0 a/\varepsilon_a$, and ρU^2 as the characteristic length, velocity, time, electrical potential, and pressure scales. The procedure introduces nine dimensionless parameters as listed in Table I. Then, we perturb the dimensionless base-state

TABLE I. The definition of dimensionless parameters.

Dimensionless parameter	Definition
Density ratio of the gas to the liquid	$\bar{\rho} = \rho_a/\rho$
Reynolds number	$\text{Re} = \rho U a/\mu$
Weber number	$\text{We} = \rho U^2 a/\gamma$
Deborah number	$\text{De} = \lambda_1 U/a$
Dimensionless elastic tension	$\text{Te} = \tau_0/\rho U^2$
Rheological time ratio	$\tilde{\lambda} = \lambda_2/\lambda_1$
Dimensionless electrostatic force	$\text{Ge} = Q_0^2/\rho U^2 \varepsilon_a$
Dimensionless electrical relaxation time	$\alpha = a\sigma/\varepsilon U$
Dielectric constant of the liquid	$\bar{\varepsilon} = \varepsilon/\varepsilon_a$

solutions with small disturbances in the form of the normal mode:

$$f = \bar{f} + \hat{f}(r)\exp(st + im\theta + ikz), \quad (18)$$

where f represents arbitrary dimensionless physical quantities, s is the eigenfrequency of disturbance with azimuthal wave number m and axial wave number k .

The dimensionless governing equations for the gas layer are then linearized as below:

$$\frac{d^2\hat{\phi}_a}{dr^2} + \frac{1}{r}\frac{d\hat{\phi}_a}{dr} - \left(\frac{m^2}{r^2} + k^2\right)\hat{\phi}_a = 0, \quad (19)$$

$$\frac{d\hat{u}_{r,a}}{dr} + \frac{\hat{u}_{r,a}}{r} + i\left(\frac{m}{r}\hat{u}_{\theta,a} + k\hat{u}_{z,a}\right) = 0, \quad (20)$$

$$\{\hat{u}_{r,a}, \hat{u}_{\theta,a}, \hat{u}_{z,a}\} = -\frac{1}{s\bar{\rho}}\left\{\frac{d\hat{P}_a}{dr}, \frac{im}{r}\hat{P}_a, ik\hat{P}_a\right\}. \quad (21)$$

Note that Eq. (19) is a modified Bessel equation in terms of $\hat{\phi}_a$, which has a solution subject to the condition of finite

physical quantities at $r = \infty$:

$$\hat{\phi}_a(r) = A_1 K_m(kr), \quad (22)$$

where A_1 is an integration constant and K_m is the m th-order modified Bessel function of the second kind. Combining Eqs. (20) and (21) gives a modified Bessel equation in terms of pressure, which also yields a solution:

$$\hat{P}_a(r) = A_2 K_m(kr), \quad (23)$$

where A_2 is an integration constant. Substituting this solution into Eq. (21), the velocity field for the ambient gas can be obtained as

$$\{\hat{u}_{r,a}, \hat{u}_{\theta,a}, \hat{u}_{z,a}\} = -\frac{A_2}{s\bar{\rho}}\left\{\frac{dk_m(kr)}{dr}, \frac{im}{r}K_m(kr), ikK_m(kr)\right\}. \quad (24)$$

For the liquid jet, the linearized perturbation equations are

$$\frac{d^2\hat{\phi}}{dr^2} + \frac{1}{r}\frac{d\hat{\phi}}{dr} - \frac{m^2}{r^2}\hat{\phi} - k^2\hat{\phi} = -\frac{\hat{q}}{\bar{\varepsilon}}, \quad (25)$$

$$(s + \alpha + ik)\hat{q} = 0, \quad (26)$$

$$\frac{d\hat{u}_r}{dr} + \frac{\hat{u}_r}{r} + \frac{im}{r}\hat{u}_\theta + ik\hat{u}_z = 0, \quad (27)$$

$$(s + ik)\hat{u}_r = -\frac{d\hat{P}}{dr} + \frac{d\hat{\tau}_{rr}}{dr} + \frac{im\hat{\tau}_{\theta r}}{r} + ik\hat{\tau}_{zr} + \frac{\hat{\tau}_{rr} - \hat{\tau}_{\theta\theta}}{r}, \quad (28)$$

$$(s + ik)\hat{u}_\theta = -\frac{im\hat{P}}{r} + \frac{d\hat{\tau}_{r\theta}}{dr} + \frac{im\hat{\tau}_{\theta\theta}}{r} + ik\hat{\tau}_{z\theta} + \frac{\hat{\tau}_{\theta r} + \hat{\tau}_{r\theta}}{r}, \quad (29)$$

$$(s + ik)\hat{u}_z = -ik\hat{P} + \frac{d\hat{\tau}_{rz}}{dr} + \frac{im\hat{\tau}_{\theta z}}{r} + ik\hat{\tau}_{zz} + \frac{\hat{\tau}_{rz}}{r}, \quad (30)$$

and

$$\hat{\tau} = \beta_1 \begin{pmatrix} 2\frac{d\hat{u}_r}{dr} & \frac{d\hat{u}_\theta}{dr} + \frac{im\hat{u}_r}{r} - \frac{\hat{u}_\theta}{r} & ik\hat{u}_r + \frac{d\hat{u}_z}{dr} \\ \frac{d\hat{u}_\theta}{dr} + \frac{im\hat{u}_r}{r} - \frac{\hat{u}_\theta}{r} & \frac{2(im\hat{u}_\theta + \hat{u}_r)}{r} & \frac{im\hat{u}_z}{r} + ik\hat{u}_\theta \\ ik\hat{u}_r + \frac{d\hat{u}_z}{dr} & \frac{im\hat{u}_z}{r} + ik\hat{u}_\theta & 2ik\hat{u}_z \end{pmatrix} + ik\beta_2 \begin{pmatrix} 0 & 0 & \hat{u}_r \\ 0 & 0 & \hat{u}_\theta \\ \hat{u}_r & \hat{u}_\theta & 2\hat{u}_z \end{pmatrix}, \quad (31)$$

with

$$\beta_1 = \frac{1}{\text{Re}} \frac{1 + \text{De}\tilde{\lambda}(s + ik)}{1 + \text{De}(s + ik)}, \quad \beta_2 = \frac{\text{DeTe}}{1 + \text{De}(s + ik)}. \quad (32)$$

Note that the term involving β_2 results from the presence of the unrelaxed elastic tension. If the stress relaxation time is extremely small (i.e., $\text{De} \rightarrow 0$), Eq. (32) gives $\beta_1 \approx 1/\text{Re}$ and $\beta_2 \approx 0$, which recovers the case of Newtonian fluid jets. Now, we use Eq. (31) to rewrite the momentum equations (28)–(30) as

$$(s + ik)\hat{u}_r = -\frac{d\hat{P}}{dr} + \beta_1 \left(\frac{d^2\hat{u}_r}{dr^2} + \frac{d\hat{u}_r}{rdr} - \frac{1 + m^2}{r^2}\hat{u}_r - k^2\hat{u}_r - 2im\frac{\hat{u}_\theta}{r^2} \right) - k^2\beta_2\hat{u}_r, \quad (33)$$

$$(s + ik)\hat{u}_\theta = -\frac{im\hat{P}}{r} + \beta_1 \left(\frac{d^2\hat{u}_\theta}{dr^2} + \frac{d\hat{u}_\theta}{rdr} - \frac{(1 + m^2)\hat{u}_\theta}{r^2} - k^2\hat{u}_\theta + 2im\frac{\hat{u}_r}{r^2} \right) - k^2\beta_2\hat{u}_\theta, \quad (34)$$

$$(s + ik)\hat{u}_z = -ik\hat{P} + \beta_1 \left(\frac{d^2\hat{u}_z}{dr^2} + \frac{d\hat{u}_z}{rdr} - \frac{m^2}{r^2}\hat{u}_z - k^2\hat{u}_z \right) - k^2\beta_2\hat{u}_z. \quad (35)$$

Since Eq. (26) implies $\hat{q} = 0$, Eq. (25) has a solution subject to finite condition at $r = 0$:

$$\hat{\phi}(r) = A_3 I_m(kr), \quad (36)$$

where A_3 is an integration constant and I_m is the m th-order modified Bessel function of the first kind.

By inspecting Eqs. (25) and (33)–(35), one can see that the electrified effects in the fluid bulk and flow motion are decoupled after linearization. In fact, the interaction between electric forces and viscoelastic stresses occurs only on the jet surface. The coupling of physical quantities at the disturbed interface, $r = 1 + \hat{\eta}e^{st+ikz+im\theta}$, can be provided by the boundary conditions (8)–(14) and their linearized forms are written as follows:

$$\bar{\epsilon} \frac{d\hat{\phi}}{dr} \Big|_{r=1} - \frac{d\hat{\phi}_a}{dr} \Big|_{r=1} - \hat{Q} - \hat{\eta} = 0, \quad (37)$$

$$\hat{\phi}(1) - \hat{\phi}_a(1) + \hat{\eta} = 0, \quad (38)$$

$$-\alpha \bar{\epsilon} \frac{d\hat{\phi}}{dr} \Big|_{r=1} + \frac{d\hat{u}_r}{dr} \Big|_{r=1} - ik\hat{Q} = s\hat{Q}, \quad (39)$$

$$\hat{u}_r(1) = (s + ik)\hat{\eta}, \quad (40)$$

$$\hat{u}_{r,a}(1) = s\hat{\eta}, \quad (41)$$

$$\hat{P}(1) - \hat{P}_a(1) - 2\beta_1 \frac{d\hat{u}_r}{dr} \Big|_{r=1} + \frac{1}{\text{We}}(1 - m^2 - k^2)\hat{\eta} - \text{Ge} \left(\bar{\epsilon} \frac{d\hat{\phi}}{dr} \Big|_{r=1} - \hat{Q} \right) = 0, \quad (42)$$

$$\beta_1 \left(ik\hat{u}_r(1) + \frac{d\hat{u}_z}{dr} \Big|_{r=1} \right) + ik\text{Ge}\hat{\phi}(1) + ik\beta_2\hat{u}_r(1) = 0, \quad (43)$$

$$\beta_1 \left(\frac{d\hat{u}_\theta}{dr} \Big|_{r=1} - \hat{u}_\theta(1) + im\hat{u}_r(1) \right) + im\text{Ge}\hat{\phi}(1) = 0. \quad (44)$$

Here Eqs. (43) and (44) account for the tangential stress balance between viscoelastic stresses (the terms involving β_1 or β_2) and electrical traction (the terms involving Ge). Additionally, the finite conditions at $r = 0$ can be written as

(i) for $m = 0$,

$$\frac{d\hat{P}}{dr} \Big|_{r=0} = 0, \quad \hat{u}_r(0) = 0, \quad \hat{u}_\theta(0) = 0, \quad \frac{d\hat{u}_z}{dr} \Big|_{r=0} = 0, \quad (45)$$

(ii) for $m = 1$,

$$\hat{P}(0) = 0, \quad \hat{u}_r(0) + i\hat{u}_\theta(0) = 0, \quad \hat{u}_z(0) = 0, \quad (46)$$

(iii) for $m \geq 2$,

$$\hat{P}(0) = 0, \quad \hat{u}_r(0) = 0, \quad \hat{u}_\theta(0) = 0, \quad \hat{u}_z(0) = 0. \quad (47)$$

C. Eigenvalue problem

The linearized equations (27) and (33)–(35) together with the boundary conditions (37)–(47) form a complicate eigenvalue problem, which is solved by the Chebyshev collocation method [28]. Note that the present analysis is restricted to the cases of $\text{We} \gg 1$ such that absolute instability does not occur. Literature indicates that for uncharged Newtonian jets, the

transition between convective and absolute instabilities occurs at about $\text{We} = 4$ [36], above which convective instability is consistent with the temporal analysis. With this restriction, we can set the axial wave number k to be a real number to determine the complex eigenfrequency, s . The real part of s (denoted by s_r) accounts for the growth rate of disturbance while the imaginary part represents the wave frequency. For a given set of parameters, only the eigenvalues with positive growth rates are collected to depict the spectrum diagrams for the unstable disturbances.

The numerical procedure firstly entails transforming the r coordinate to the ξ domain through $r = (\xi + 1)/2$, and then expanding the variables using N -terms Chebyshev polynomials as the set of basis functions:

$$\hat{P}(\xi) = \sum_{n=0}^N c_{n+1} \Psi_n(\xi), \quad (48)$$

$$\hat{u}_r(\xi) = \sum_{n=0}^N c_{N+1+n+1} \Psi_n(\xi), \quad (49)$$

$$\hat{u}_\theta(\xi) = \sum_{n=0}^N c_{2N+2+n+1} \Psi_n(\xi), \quad (50)$$

$$\hat{u}_z(\xi) = \sum_{n=0}^N c_{3N+3+n+1} \Psi_n(\xi), \quad (51)$$

where $\Psi_n(\xi) = \cos(n \cos^{-1} \xi)$. The expansion must exactly satisfy the boundary conditions at $\xi = \pm 1$ and at the interior points $\xi_j = \cos(j\pi/N)$ for $j = 1$ to $N-1$. This demand yields a quadratic eigenvalue problem:

$$\mathbf{M}\mathbf{x} = s\mathbf{K}\mathbf{x} + s^2\mathbf{D}\mathbf{x}, \quad (52)$$

where $\mathbf{x} = \{c_1, c_2, \dots, c_{4N+4}, \hat{\eta}, A_1, A_2, A_3\} \in C^{4N+8}$, and \mathbf{M} , \mathbf{K} , and \mathbf{D} are the coefficient matrices. This problem is solvable if we create the following matrix transformation:

$$\mathbf{A} = \begin{pmatrix} \mathbf{M} & \mathbf{0} \\ \mathbf{0} & \mathbf{I} \end{pmatrix}, \quad \mathbf{B} = \begin{pmatrix} \mathbf{K} & \mathbf{D} \\ \mathbf{I} & \mathbf{0} \end{pmatrix}, \quad \mathbf{v} = \begin{pmatrix} \mathbf{x} \\ s\mathbf{x} \end{pmatrix}. \quad (53)$$

Applying the transformation to Eq. (52) yields a generalized eigenvalue problem:

$$\mathbf{A}\mathbf{v} = s\mathbf{B}\mathbf{v}. \quad (54)$$

Using a common matrix algorithm with $N \approx 35$, we can obtain efficient and accurate solutions for such an eigenvalue problem. The numerical code has been validated by plotting the dispersion diagrams (i.e., the growth rate s_r against the wave numbers m and k) and comparing the results with those in previous studies for the cases with or without electrification and viscoelastic stresses. On the other hand, in the zero-tension limit (i.e., $\beta_2 = 0$), Eqs. (33)–(35) have analytic solutions, which eventually yield a dispersion relation in the form of a determinant of 8×8 matrix. Excellent agreements have been obtained for more reduced cases, which also supports the validation of the present numerical code.

IV. RESULTS AND DISCUSSIONS

A. Parametric ranges and basic dispersion diagrams

According to the literature [30,34,35], most Boger fluids have viscosities varying in the range of 10^{-3} –1 Pa s with density $\rho \approx 10^3$ kg/m³ and dielectric constant $\bar{\epsilon} \approx 10$. The stress relaxation time λ_1 varies from 10^{-2} to 10 s, depending on the polymeric molecular weight and concentration. The value of surface tension is on the order of 10^{-2} N/m, but can be further reduced by mixing surfactants into the polymeric solutions. The electrical conductivity of common polymer solutions varies in the range of $\sigma = 10^{-8}$ – 10^{-5} S/m. Generally, adding a certain amount of salts or conducting polymers into solutions can improve the conductivity up to 1 S/m or more. The axial tension τ_0 varies from 1 to 10 Pa, estimated via the formulation proposed by Bousfield *et al.* [26] for a capillary tube of diameter $d_0 \approx 1$ mm. If we consider that the jet has a radius $a \approx 10^{-4}$ m, surface charge density $Q_0 \approx 10^{-5}$ C/m², and moves at velocity $U = 1$ –10 m/s through the gas medium of $\rho_a \approx 1$ kg/m³; the parametric ranges can be estimated as follows: $Re = 10^{-1}$ – 10^3 , $We = 10$ – 10^3 , $\bar{\rho} \approx 10^{-3}$, $Ge = 10^{-4}$ –0.1, $\alpha = 10^{-1}$ – 10^8 , $De = 10^2$ – 10^6 , $Te = 10^{-5}$ – 10^{-2} . Moreover, the rheological time ratio $\tilde{\lambda}$ must be smaller than 1 and usually varies from 0.1 to 0.5 [21,22,25]. Therefore, we

choose

$$[Re, We, \bar{\rho}, Ge, \alpha, \bar{\epsilon}, De, \tilde{\lambda}, Te] = [10, 10^2, 10^{-3}, 0.03, 10^3, 10, 10^4, 0.5, 0.002] \quad (55)$$

as the basic case for consideration. This case is relevant to a charged jet of Boger fluids moving through the air. Based on this case, we show dispersion diagrams for several limiting cases in Fig. 2.

Firstly, Fig. 2(a) illustrates the case of uncharged Newtonian jets obtained by setting $Ge = De = Te = 0$. In this case, only the axisymmetric disturbances with axial wave number smaller than 1 can grow, which allows the jet to break up into a stream of drops of diameter comparable to the circumference of the unperturbed jet. As the jet is electrified to a certain extent as shown in Fig. 2(d), the long-wavelength axisymmetric disturbances are suppressed while the short-wavelength ones are triggered. Particularly, the nonaxisymmetric sinuous mode ($m = 1$) has growth rates much higher than that of the axisymmetric mode, allowing a bending motion to develop and eventually causing the so-called bending instability observed in most experiments of electrified jets. Figures 2(b) and 2(e) illustrate the cases of viscoelastic jet in the absence of the unrelaxed tension i.e. ($Te = 0$). Carefully comparing Figs. 2(b) and 2(e) with Figs. 2(a) and 2(d), we find that the growth rates of disturbances of viscoelastic jets are less stable than those of their Newtonian counterparts no matter whether

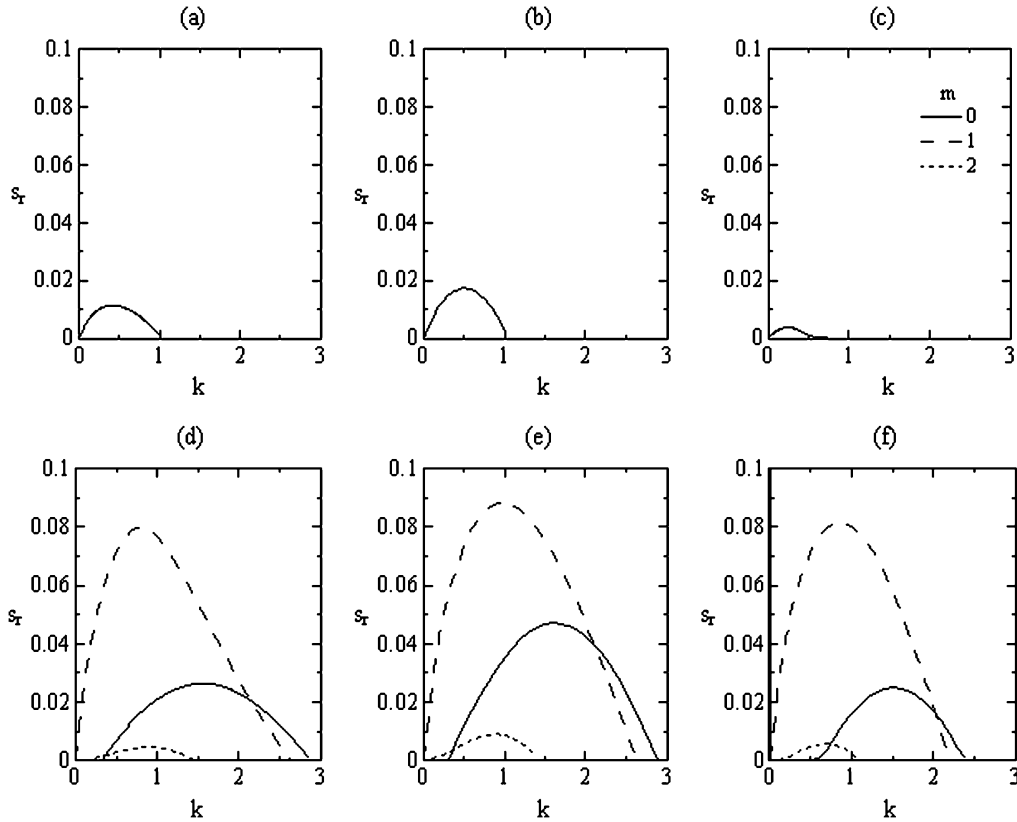


FIG. 2. The growth rate s_r vs the axial wave number k for the cases using the parameters listed in Eq. (55): (a) Uncharged Newtonian jet ($Ge = De = Te = 0$), (b) uncharged viscoelastic jets without unrelaxed tension ($Ge = Te = 0$), (c) uncharged viscoelastic jet, (d) electrified Newtonian jet ($Te = De = 0$), (e) electrified viscoelastic jet without unrelaxed tension ($Te = 0$), (f) electrified viscoelastic jet with nonzero axial tension.

the jet is electrified or not. Because the difference between the viscoelastic and Newtonian cases in the figures is not obvious, we list the maximum growth rate, $s_{r\max}$, and the corresponding wave number k_{\max} for each unstable mode in Table II to manifest this difference. It is seen that the maximum growth rate and the related axial wave number of the most dangerous disturbance for the viscoelastic jets with $Te = 0$ are larger than those for the Newtonian jets. For example, the $s_{r\max}$ of the case in Fig. 2(b) is 0.0174 larger than the value in Fig. 2(a), 0.0115. This result implies that the elastic force has a destabilizing effect on the onset of instability. However, once the unrelaxed axial tension increases to a certain magnitude, both the cutoff wave numbers and the growth rate of disturbances will decrease as shown in Figs. 2(c) and 2(f). In this situation, the elasticity becomes a factor that suppresses the growth of disturbances.

After examining more cases, we found that the reduction in the growth rate of the most dangerous disturbance for the sinuous mode ($m = 1$) is not as drastic as those for the other modes, thus relatively promoting the sinuous disturbances. The phenomenon should be responsible for the bending motion observed in experiments. The physical reason for the bending instability caused by electrification can be briefly explained via a faked “spring-damping-bead” configuration, which was first introduced by Reneker [37] to replace the real flow motion equivalently in a segment of a charged polymer jet as demonstrated in Fig. 3. In this faked system, each two adjoining rigid balls, carrying unequal charges, are connected by a string and a damper in series. We suppose that the system is subjected to a small perturbation; this causes the middle ball to slightly depart from its initial unperturbed position. The electrostatic repulsive forces provided by the adjoining balls yield a transverse component F_e which keeps on pushing the middle ball outward. As the transverse displacement increases, the strength of the outward resultant force rises and thus enhances the perturbation. Meanwhile, the aerodynamic drag F_a is always opposite to the flow; the surface tension force F_s , acting as an inward transverse force, suppresses the amplification of the perturbation; the viscoelastic forces F_v caused by the stretching of springs and dampers also provide resistance to the transverse motion. In summary, the electrical force and the aerodynamic drag provide destabilizing mechanisms, while the viscoelastic forces

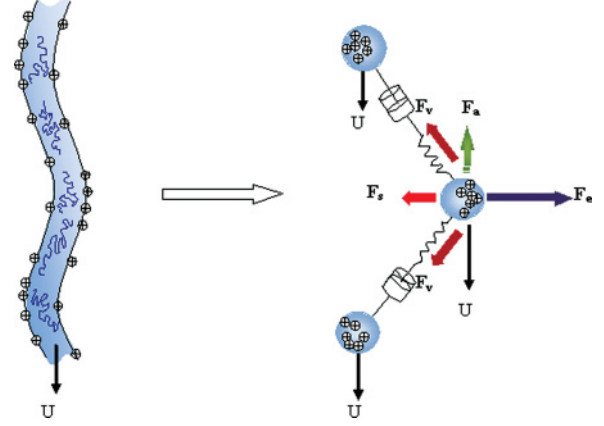


FIG. 3. (Color online) Mechanisms analysis for the growth of the sinuous mode. The segment of a charged polymer jet is supposed to be a spring-damping-bead system, in which the resultant electric force (F_e) and the aerodynamic drag (F_a) appear to enhance the perturbation, while the viscoelastic force (F_v) and surface tension (F_s) provide resistance to the transverse motion. The unbalanced forces yield a bending moment that twists the segment.

and surface tension have stabilizing effects. Nevertheless, due to the asymmetry of forces, a bending moment is inevitably generated to twist the system especially when the elongations of the strings are nonuniform. Such a resultant moment will greatly enhance the perturbation and finally cause the bending instability.

B. Elucidation of physical mechanisms via parametric study

Although the mechanical analysis via the faked spring-damping-bead system has provided a logical explanation for the cause of the bending instability, some instability behaviors such as the phenomena associated with the beads-on-string structure are still not clearly understood. Actually, the physical mechanisms in the real flow system exhibit a complex interaction much more than those described in the faked system. This section aims to investigate the individual effect of each physical parameter on the jet instability. The variations of the maximum growth rate and the corresponding axial wave

TABLE II. The information of the most dangerous disturbance of each unstable mode for the cases illustrated in Fig. 2.

Type of jet	Mode	$s_{r\max}$	k_{\max}
Figure 2(a): Uncharged Newtonian jet	$m = 0$	0.0115	0.41
Figure 2(b): Uncharged viscoelastic jet ($Te = 0$)	$m = 0$	0.0174	0.50
Figure 2(c): Uncharged viscoelastic jet ($Te = 0.002$)	$m = 0$	0.0039	0.24
	$m = 0$	0.0264	1.56
Figure 2(d): Electrified Newtonian jet	$m = 1$	0.0797	0.81
	$m = 2$	0.0046	0.88
	$m = 0$	0.0472	1.60
Figure 2(e): Electrified viscoelastic jet ($Te = 0$)	$m = 1$	0.0884	1.00
	$m = 2$	0.0090	0.92
	$m = 0$	0.0250	1.50
Figure 2(f): Electrified viscoelastic jet ($Te = 0.002$)	$m = 1$	0.0815	0.91
	$m = 2$	0.0056	0.70

number are examined based on the basic case [i.e., Eq. (55)] in a wide parameter space so as to elucidate the instability nature of physical mechanisms.

1. Surface tension (effect of the Weber number)

Surface tension is a mechanism that tends to minimize the surface area of liquid, thus having the capability of suppressing the growth of nonaxisymmetric disturbances and simultaneously enhancing the axisymmetric disturbances with axial wave number smaller than 1. Incipient theoretical works [3] have indicated that if an un electrified capillary jet is subjected to surface-tension instability only, it tends to axisymmetrically disintegrate into a stream of drops of diameter comparable to the circumference of the unperturbed jet. In this paper, surface tension is characterized by the Weber number We . An increase in We implies a decrease in surface tension. The surface tension for a liquid can be adjusted by either adding surfactants or mixing a different percentage of solvents such as ethanol. Once the surface tension declines, other mechanisms will be promoted relatively and then cause a change in the type of instability. Figure 4 depicts the variations in the $s_{r,max}$ and k_{max} with We for each unstable mode due to a change in surface tension. Note that more nonaxisymmetric modes with larger azimuthal wave numbers growing with We are not shown in the figure for simplification. At low We , the surface tension

prevails over the other destabilizing mechanisms, causing the predominance of long-wavelength axisymmetric disturbances. As We increases, the growth rate of axisymmetric disturbances decreases, while the short-wavelength disturbances begin to emerge because of the stimulation by electrostatic forces. Note that the maximum growth rate $s_{r,max}$ of the axisymmetric mode encounters a minimum value occurring at about $We = 56$. This value is associated with $GeWe \approx 1$, implying that the electrical forces are expected to overcome the surface tension. At a larger value of We the aerodynamic interaction also overcomes the surface tension and destabilizes the system by triggering more modes with higher axial and azimuthal wave numbers.

In view of practical applications such as continuous ink-jet printing, the axisymmetric breakup is desired for creating uniform charged drops. On the other hand, the technology involving the production of uniform and continuous thin fibers must avoid the growth of axisymmetric disturbances as far as possible because it is responsible for the formation of the beads-on-string structure. Adding surfactants into polymer solutions for reducing surface tension seems to be a feasible way to suppress the growth of axisymmetric disturbances. Nevertheless, according to the results illustrated in Fig. 4, the amount of surfactant must be controlled in a certain range to achieve good inhibition. The main reason is that an excessively low surface tension may relatively promote the electrical force, resulting in the growth of shorter-wavelength axisymmetric disturbances. Only when the surface tension is adjusted to a certain extent that the axisymmetric mode is stable much more than other modes can one efficiently suppress the formation of beads.

2. Aerodynamic interaction (effect of the density ratio)

The aerodynamic interaction, arising from the relative motion between the jet and the gas, is another factor that amplifies disturbances [38–40]. In this paper, the aerodynamic interaction is characterized by $\bar{\rho}$. For an uncharged Newtonian fluid jet, the onset of nonaxisymmetric disturbances can occur only when the aerodynamic drag overcomes the surface tension (i.e., $\bar{\rho} We > 1$) if no other mechanism such as swirling effect comes in to act together. In most experiments of electrified viscoelastic jets, the value of $\bar{\rho} We$ is smaller than unity and thus the aerodynamic interaction is insignificant relative to the electrified effects. As shown in Fig. 5, the growth rates of disturbances for $\bar{\rho} = 0.003$ are slightly higher than those for $\bar{\rho} = 0$. Figure 6 shows that as $\bar{\rho}$ increases, a significant amplification can be predicted and some modes with higher azimuthal wave number can be stimulated by aerodynamic effect by increasing $\bar{\rho}$ up to 0.025, which is relevant to a gas pressure of 25 atm. Therefore, the aerodynamic interaction in normal atmospheric conditions is safely negligible for the onset of instability. Nevertheless, the aerodynamic drag could become significant when the jet encounters large nonlinear deformation.

3. Electrical mechanisms

Electrical effects in the present problem include the relaxation of free charges and the influences of dielectric constant and the electrical stresses, which are characterized respectively

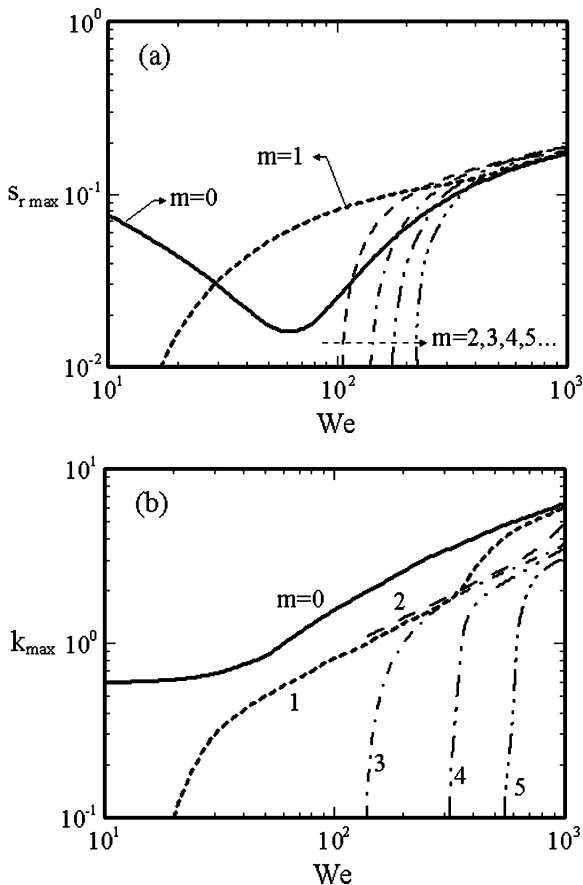


FIG. 4. The variation in (a) $s_{r,max}$, (b) k_{max} with the Weber number We for each unstable mode in the basic case.

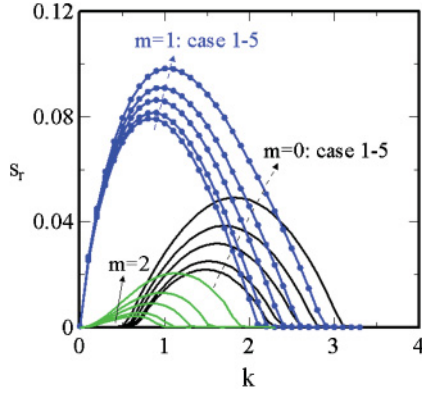


FIG. 5. (Color online) The growth rate vs the axial wave number for the cases 1: $\bar{\rho} = 0$; 2: $\bar{\rho} = 0.001$; 3: $\bar{\rho} = 0.003$; 4: $\bar{\rho} = 0.005$; 5: $\bar{\rho} = 0.008$.

by α , $\bar{\epsilon}$, and Ge . As illustrated in Sec. IV A, electrification stimulates the growth of nonaxisymmetric disturbances with short wavelength because the electrical stresses acting on the liquid surface tend to destabilize the flow in such a manner that the total electrical potential is minimized fastest. If the electrical relaxation time is infinitely small, the response of deformation to the transport of charges is instantaneous. On the contrary, if the liquid is of poor conductivity, the finite electrical relaxation time will delay the growth of disturbances. López-Herrera *et al.* [13] had performed an axisymmetric

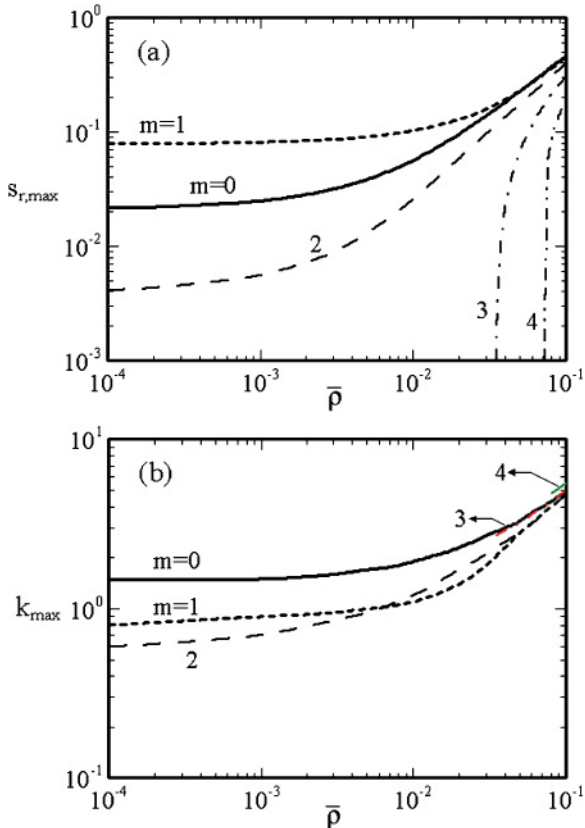


FIG. 6. The variation in (a) $s_{r,max}$, (b) k_{max} with the density ratio $\bar{\rho}$ for each unstable mode in the basic case.

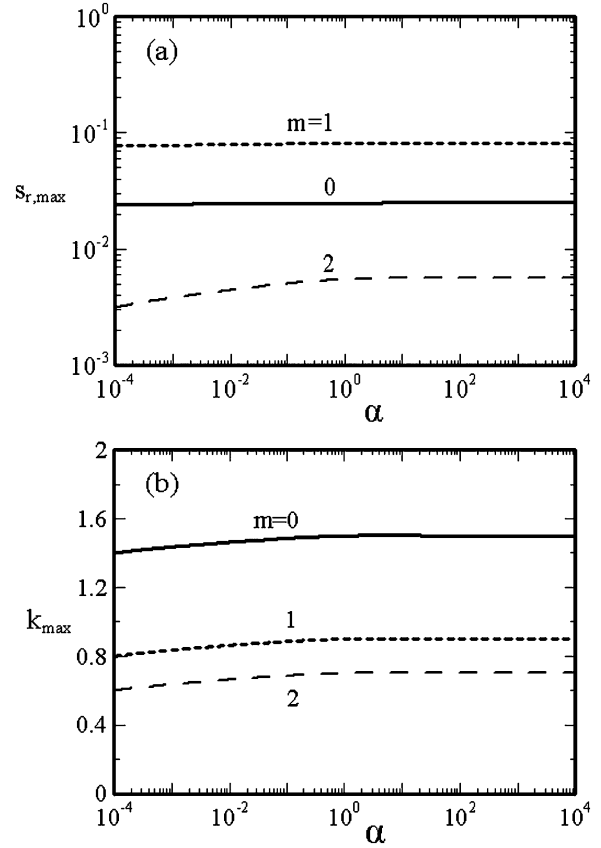


FIG. 7. The variation in (a) $s_{r,max}$, (b) k_{max} with the dimensionless electrical relaxation time α for each unstable mode in the basic case.

instability analysis for a charged Newtonian jet. Their results show that a perfectly conducting liquid jet is less stable than a dielectric fluid jet and the growth rate increases with an increasing dielectric constant. In the present analysis, we use the following parameters, $[Re, We, \bar{\rho}, Ge, \bar{\epsilon}, De, \bar{\lambda}, Te] = [10, 100, 10^{-3}, 0.006, 2, 0, 0, 0]$, to fit their result and get good agreement. However, when we increase the electrical force to $Ge = 0.03$, the influence of α on the maximum growth rate becomes negligible as shown in Fig. 7. This result implies that the effect of charge transport is important only when the charge amount is not high.

To illustrate the effect of electrical force, we depict in Fig. 8 the variations of $s_{r,max}$ and k_{max} with Ge for each unstable mode based on the basic case. It is noted that when Ge is small, the surface tension dominates the instability and only the axisymmetric mode grows. As Ge increases, the electrical force gradually overcomes the surface tension and lowers the axisymmetric mode. The nonaxisymmetric mode $m = 1$ first merges at about $Ge = 0.002$, and then the other modes with higher azimuthal wave numbers appear in sequence at larger values of Ge and rapidly rise to dominate the instability in terms of the disturbances with higher axial wave number. In particular, the curve of $s_{r,max}$ for the axisymmetric mode possesses a minimum approximately at $Ge = 0.01$ (or $GeWe = 1$), where the electrical force balances off the surface tension due to the same physical mechanism as that discussed in Fig. 4. We also note that the k_{max} of $m = 1$ increases with increasing Ge , implying that the whipping

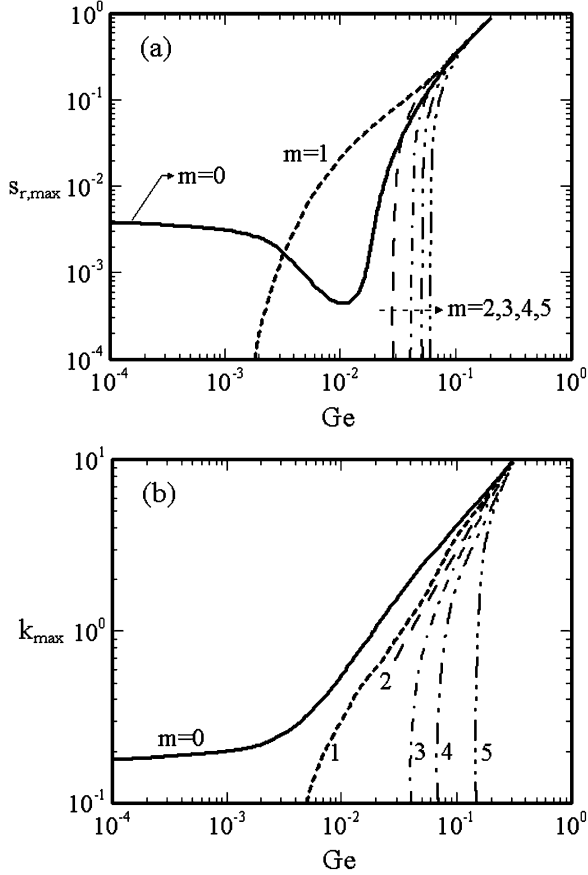


FIG. 8. The variation in (a) $s_{r,max}$, (b) k_{max} with the dimensionless electric force Ge for each unstable mode in the basic case.

wavelength will be shortened once the amount of charges increases.

4. Viscoelastic effects

Viscoelastic effects include viscous damping and the relaxation and storage of elastic energy. The viscous damping, characterized by Re , is a mechanism that stabilizes the flow by dissipating the kinetic energy of disturbances. According to the studies on the instability of uncharged Newtonian jets [38,40], an increase in viscosity significantly reduces the growth rates of axisymmetric and nonaxisymmetric disturbances. Nevertheless, the damping effect for the sinuous mode is relatively weak compared with the other modes. In certain conditions, the sinuous mode may become predominant even for unelectrified jets due to the bending moment induced by the nonuniform distribution of the viscous forces. Figure 9 illustrates the effect of Reynolds number on the instability behaviors. It is found that when the Reynolds number decreases, the growth rate of the sinuous mode $m = 1$ diminishes slightly but the modes $m = 0$ and $m = 2$ decrease rapidly. As a result, an increase in the liquid viscosity can be expected to eliminate the formation of beads efficiently but promote the long-wavelength sinuous motion relatively.

The fluid elasticity can play a destabilizing or stabilizing role depending on whether it relaxes or stores the kinetic energy. For a weakly elastic liquid (i.e., $De < 100$), the stress

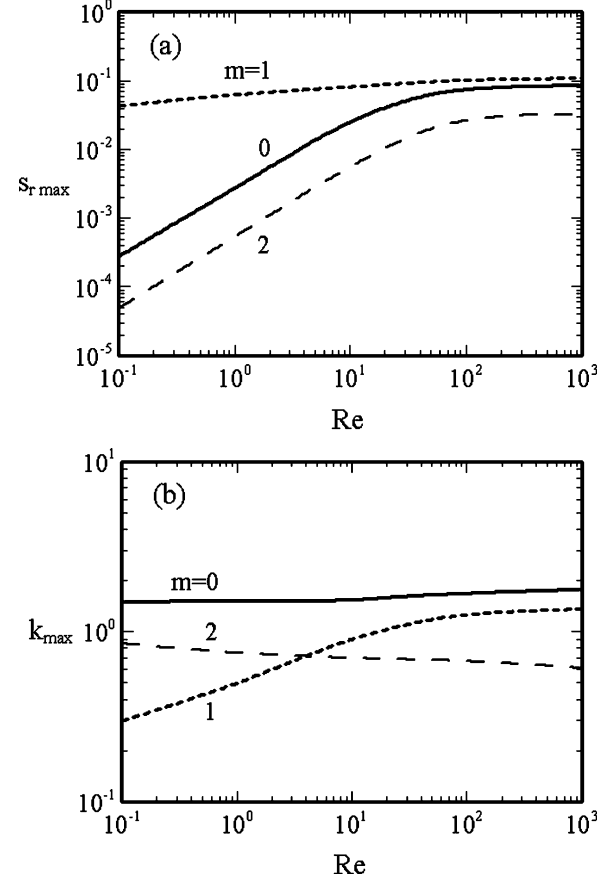


FIG. 9. The variation in (a) $s_{r,max}$, (b) k_{max} with the Reynolds number Re for each unstable mode in the basic case.

relaxation time is small such that the elastic stress generated at the capillary tube can relax immediately after ejection from the nozzle (i.e., $Te = 0$). On the other hand, for a viscoelastic jet with high De , the unrelaxed tension can persist for a long distance from the nozzle exit and inevitably affect the flow motion.

Note that in Sec. III A, we have restricted $De \gg 1$ to obtain a constant initial elastic tension in order that the instability analysis is feasible. Figure 10 shows the variations of $s_{r,max}$ and k_{max} with Te for each unstable mode. As seen in this figure, although the modes $m = 0$ and $m = 2$ are greatly suppressed with increasing Te , the growth rate of the sinuous mode $m = 1$ is almost unchanged but the wavelength of the most unstable disturbance is elongated. Consequently, an increase in the fluid elasticity relatively promotes the predominance of sinuous disturbance.

The last parameter considered is to examine the effect of the rheological time ratio $\tilde{\lambda}$ which actually represents the deformation retardation time if the number De is held constant. Physically, the deformation retardation time accounts for the response of strain to viscoelastic stresses. When the retardation time is long, the response speed is slow and thus delays the deformation. Indeed, our numerical calculation shows that an increase in $\tilde{\lambda}$ has a stabilizing effect on the instability as displayed in Fig. 11. Here again, changing the time ratio merely affects the sinuous mode slightly and the related instability characteristics are quite similar as the results illustrated in

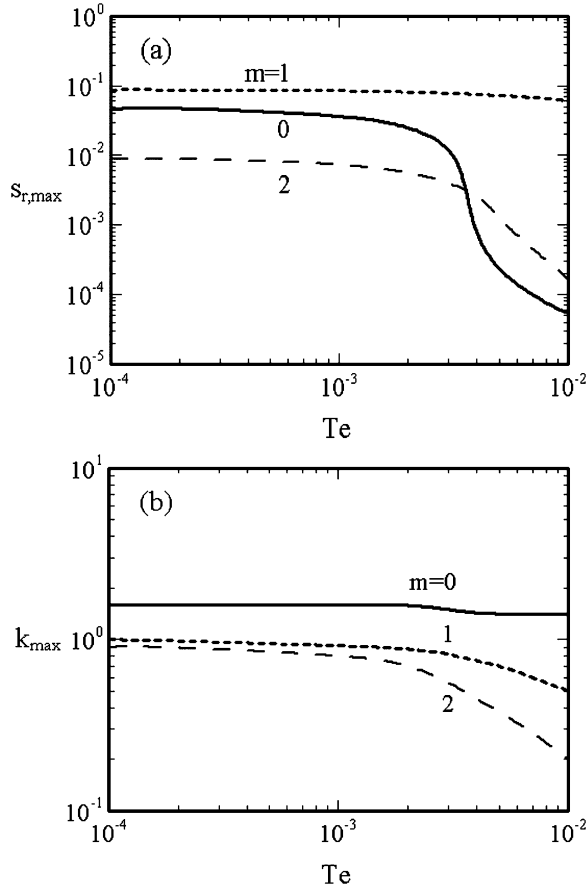


FIG. 10. The variation in (a) $s_{r,max}$, (b) k_{max} with Te for each unstable mode in the basic case.

Figs. 9 and 10. In summary, an increase in either the viscosity or the elasticity will greatly suppress the formation of beads and simultaneously promote the bending motion in electrified viscoelastic jets.

V. CONCLUSIONS

We have performed a detailed three-dimensional instability analysis of a charged non-Newtonian jet. In the present study, we employ the Oldroyd-B equation to describe the viscoelastic behavior and use the leaky-dielectric model to account for the charge transport process. The resultant eigenvalue problem was solved by the Chebyshev collocation method with a matrix transformation. The coupling between the electrical forces, viscoelastic stresses, surface tension, and aerodynamic interaction was completely investigated via a series of parametric analysis. The instability features are summarized as follows:

(1) Electrification inherently enhances the growth of axisymmetric and nonaxisymmetric disturbances with shorter wavelengths. In most situations, the sinuous mode has the largest growth rate, which is responsible for the bending motion developing downstream of the jet.

(2) While viscous damping stabilizes the jet by dissipating the kinetic energy of disturbances, elastic stresses appear to suppress the growth of disturbances by restoring and relaxing

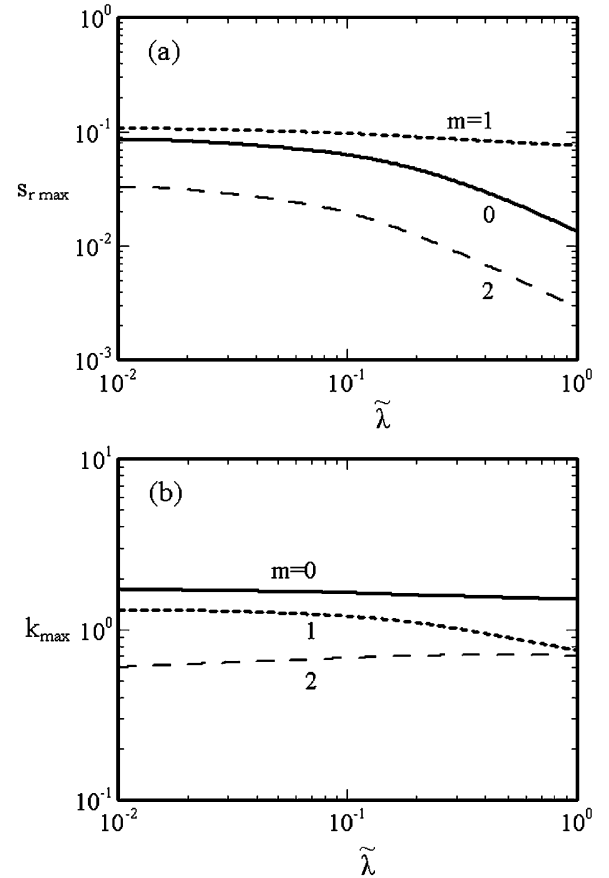


FIG. 11. The variation in (a) $s_{r,max}$, (b) k_{max} with the rheological time ratio $\tilde{\lambda}$ for each unstable mode in the basic case.

elastic energy. This implies that an increase in the polymer concentration can efficiently delay the breakup of jets.

(3) Surface tension is the key mechanism that prefers to enhance axisymmetric disturbances with wavelength comparable to the jet circumference while suppressing all of the non-axisymmetric disturbances. The growth of the axisymmetric mode is responsible for the formation of the beads-on-strings structure. Decreasing surface tension has been regarded as a feasible way to suppress the formation of beads. However, excessively low surface tension may relatively promote the electrical force to amplify the short-wavelength axisymmetric disturbances. As a result, only when the electrical force balances off the surface tension, can the beads be eliminated completely.

(4) Aerodynamic interaction, arising from the relative motion between the jet and the surrounding gas, has a purely destabilizing effect on the instability. However, in the presence of electrical stresses, its effect becomes relatively insignificant.

The present analysis has provided a fundamental understanding of the instability phenomena occurring in electrified viscoelastic jets. However, these results are restricted to the cases associated with jets driven by hydrodynamic pressure, which are applicable mainly for continuous ink-jet printing. For technologies involving the production of nanofibers or microdroplets via electrically driven jets ejected from the so-called Taylor cone, the effect of axial electric field must

be taken into account. In the future, a three-dimensional instability analysis coupled with the effect of axial electric field on the flow field in the Taylor cone should be an imperative work that benefits the development of electrified jet technology.

ACKNOWLEDGMENTS

This work is supported by funding from the National Science Council of Taiwan through Grant No. NSC 99-2221-E-002-083-MY3.

-
- [1] R. H. Magarvey and L. E. Outhouse, *J. Fluid Mech.* **13**, 151 (1962).
- [2] M. Cloupeau and B. Prunet-Foch, *J. Electrostatics* **25**, 165 (1990).
- [3] L. Rayleigh, *Philos. Mag.* **14**, 184 (1882).
- [4] A. B. Basset, *Am. J. Math.* **16**, 93 (1894).
- [5] G. I. Taylor, *Proc. R. Soc. London, Ser. A* **313**, 453 (1969).
- [6] J. M. Schneider, N. R. Lindblad, C. D. Hendricks, and J. M. Crowley, *J. Appl. Phys.* **38**, 2599 (1967).
- [7] A. L. Huebner, *J. Fluid Mech.* **38**, 679 (1969).
- [8] A. L. Huebner, *Science* **168**, 118 (1970).
- [9] A. L. Huebner, *J. Fluid Mech.* **49**, 361 (1971).
- [10] D. A. Saville, *Phys. Fluids* **14**, 1095 (1971).
- [11] D. A. Saville, *Annu. Rev. Fluid Mech.* **29**, 27 (1997).
- [12] J. R. Melcher and G. I. Taylor, *Annu. Rev. Fluid Mech.* **1**, 111 (1969).
- [13] J. M. López-Herrera, P. Riesco-Chueca, and A. M. Gañán-Calvo, *Phys. Fluids* **17**, 034106 (2005).
- [14] F. Li, X.-Y. Yin, and X.-Z. Yin, *J. Fluid Mech.* **596**, 285 (2008).
- [15] F. Li, X.-Y. Yin, and X.-Z. Yin, *J. Fluid Mech.* **632**, 199 (2009).
- [16] A.-C. Ruo, M.-H. Chang, and F. Chen, *Phys. Fluids* **22**, 044102 (2010).
- [17] O. A. Basaran, *AIChE J.* **48**, 1842 (2002).
- [18] B.-J. de Gans, P. C. Duineveld, and U. S. Schubert, *Adv. Mater.* **16**, 203 (2004).
- [19] S. Middleman, *Chem. Eng. Sci.* **20**, 1037 (1965).
- [20] F. W. Kroesser and S. Middleman, *AIChE J.* **15**, 383 (1969).
- [21] G. Brenn, Z. Liu, and F. Durst, *Int. J. Multiphase Flow* **26**, 1621 (2000).
- [22] Z. Liu and Z. Liu, *J. Fluid Mech.* **559**, 451 (2006).
- [23] M. Goldin, J. Yerushalmi, R. Pfeffer, and R. Shinnar, *J. Fluid Mech.* **38**, 689 (1969).
- [24] M. Gordon, J. Yerushalmi, and R. Shinnar, *J. Rheol.* **17**, 303 (1973).
- [25] S. L. Goren and M. Gottlieb, *J. Fluid Mech.* **120**, 245 (1982).
- [26] D. W. Bousfield, R. Keunings, G. Marrucci, and M. M. Denn, *J. Non-Newtonian Fluid Mech.* **21**, 79 (1986).
- [27] R. B. Bird, R. C. Armstrong, and O. Hassager, *Dynamics of Polymeric Liquids*, 2nd ed., Vol. 1 (Wiley, New York, 1987).
- [28] J. P. Boyd, *Chebyshev and Fourier Spectral Methods* (Springer, New York, 1989).
- [29] R. G. Larson, *Rheol. Acta* **31**, 213 (1992).
- [30] D. F. James, *Annu. Rev. Fluid Mech.* **41**, 129 (2009).
- [31] R. B. Bird and J. M. Wiest, *Annu. Rev. Fluid Mech.* **27**, 169 (1995).
- [32] D. V. Boger, *J. Non-Newtonian Fluid Mech.* **3**, 87 (1977).
- [33] R. J. Binnington and D. V. Boger, *J. Rheol.* **29**, 887 (1985).
- [34] R. P. Mun, J. A. Byars, and D. V. Boger, *J. Non-Newtonian Fluid Mech.* **74**, 285 (1998).
- [35] J. H. Yu, S. V. Fridrikh, and G. C. Rutledge, *Polymer* **47**, 4789 (2006).
- [36] S.-P. Lin and Z.-W. Lian, *Phys. Fluids A* **1**, 490 (1989).
- [37] D. H. Reneker, A. L. Yarin, H. Fong, and S. Koombhongse, *J. Appl. Phys.* **87**, 4531 (2000).
- [38] X.-G. Li, *Atomization Sprays* **5**, 89 (1995).
- [39] E. Avital, *Phys. Fluids* **7**, 1162 (1995).
- [40] A.-C. Ruo, M.-H. Chang, and F. Chen, *Phys. Fluids* **20**, 062105 (2008).